Biomaterials 284 (2022) 121494

Contents lists available at ScienceDirect

Biomaterials

journal homepage: www.elsevier.com/locate/biomaterials

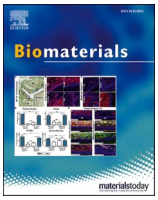

Impact of the multiscale viscoelasticity of quasi-2D self-assembled protein networks on stem cell expansion at liquid interfaces

Dexu Kong [a,b,1], Lihui Peng [a,b,1], Minerva Bosch-Fortea [a,b], Alexandra Chrysanthou [a,b], Cardee V.J-M. Alexis [a,b], Carlos Matellan [c], Ali Zarbakhsh [d], Giulia Mastroianni [d], Armando del Rio Hernandez [c], Julien E. Gautrot [a,b,*]

[a] Institute of Bioengineering, Queen Mary, University of London, Mile End Road, London, E1 4NS, UK
[b] School of Engineering and Materials Science, Queen Mary, University of London, Mile End Road, London, E1 4NS, UK
[c] Cellular and Molecular Biomechanical Laboratory, Department of Bioengineering, Imperial College London, SW7 2AZ, UK
[d] School of Biological and Chemical Sciences, Queen Mary, University of London, Mile End Road, London, E1 4NS, UK

ARTICLE INFO

Keywords:
2D nanomaterials
Protein nanosheet
Self-assembly
Viscoelasticity
Stem cells
Liquid-liquid interface

ABSTRACT

Although not typically thought to sustain cell adhesion and expansion, liquid substrates have recently been shown to support such phenotypes, providing protein nanosheets could be assembled at corresponding liquid-liquid interfaces. However, the precise mechanical properties required from such quasi-2D nanoassemblies and how these correlate with molecular structure and nanoscale architecture has remained unclear. In this report, we screen a broad range of surfactants, proteins, oils and cell types and correlate interfacial mechanical properties with stem cell expansion. Correlations suggest an impact of interfacial viscoelasticity on the regulation of such behaviour. We combine interfacial rheology and magnetic tweezer-based interfacial microrheology to characterise the viscoelastic profile of protein nanosheets assembled at liquid-liquid interfaces. Based on neutron reflectometry and transmission electron microscopy data, we propose that the amorphous nanoarchitecture of quasi-2D protein nanosheets controls their multi-scale viscoelasticity which, in turn, correlates with cell expansion. This understanding paves the way for the rational design of protein nanosheets for microdroplet and bioemulsion-based stem cell manufacturing and screening platforms.

1. Introduction

Stem cell technologies are revolutionising the fields of regenerative medicine, biotherapeutics production and advanced *in vitro* tissue culture models [1–4]. The associated expansion in the number of cell lines to be generated, maintained and differentiated (e.g. developed by cell banks, or associated with next generation cell assay-based screening) requires novel technologies to increase the throughput and scale up of cell culture [5]. This has led to the development of a range of 3D bioreactors, from hollow fibre systems to solid microcarriers [6,7]. However, such systems remain limited in terms of processability, scalability and cost of production. Inspired by the success of emulsion-based platforms in the field of chemical engineering, for flow through chemistry and microdroplet technologies [8,9], microdroplet bioreactors have recently been proposed to replace solid microcarriers for the culture of adherent stem cells [10]. Indeed, microdroplet-based platforms are based on inexpensive oils that can be separated easily from cell products and be recycled, without leaving plastic microparticles in resulting products.

At first glance, such paradigm shift contrasts with the importance of the mechanical properties of biomaterials to regulate stem cell adhesion, expansion and phenotype [11,12]. Yet, the culture of stem cells at the surface of liquids and the retention of their phenotype was recently reported to be mediated by the self-assembly of protein nanosheets at liquid-liquid interfaces [10,13–15]. These assemblies are associated with increases in interfacial shear moduli by orders of magnitude, compared to pristine liquid-liquid interfaces [13,16]. However, the factors controlling the molecular structure of these assemblies, their impact on interfacial mechanics and, in turn, the regulation of cell expansion remained largely unknown.

* Corresponding author. Institute of Bioengineering, Queen Mary, University of London, Mile End Road, London, E1 4NS, UK.
E-mail address: j.gautrot@qmul.ac.uk (J.E. Gautrot).
[1] Contributed equally to this work.

https://doi.org/10.1016/j.biomaterials.2022.121494
Received 14 December 2021; Received in revised form 23 March 2022; Accepted 28 March 2022
Available online 6 April 2022
0142-9612/© 2022 The Authors. Published by Elsevier Ltd. This is an open access article under the CC BY license (http://creativecommons.org/licenses/by/4.0/).

Indeed, although the adsorption of albumin nanosheets increases the interfacial shear modulus of fluorinated oil-aqueous interfaces 743-fold (underestimate due to the lack of viscous drag correction), this was found to be insufficient to support the culture of epithelial cells (HaCaT cells) [13]. The introduction of pentafluoro benzoyl chloride (PFBCl) within such systems (in the bulk oil) enabled the formation of large epithelial colonies, despite a further increase in interfacial modulus by a factor of only 2.2. Such a striking impact of interfacial mechanics on cell expansion contrasts with the broader range of mechanics of hydrogels and soft-matter substrates to which cells typically respond [17,18]. The impact of surfactant chemistry (as in PFBCl) on nanosheet assembly and mechanics, although reported to be important to enable cell culture [19], remains unclear too. Similarly, switching the oil from perfluorodecalin to perfluorooctane had a striking impact on mesenchymal stem cell adhesion and phenotype [14], whereas silicone oils with a broad range of viscosities did not impact cell expansion significantly [16]. Overall, cell phenotype (e.g. adhesion, expansion, colony formation and differentiation) was found to be modulated particularly strongly by relatively modest changes in interfacial moduli, implying that other physical and mechanical interfacial properties may contribute to regulate cell response to changes in liquid-liquid interfaces. Therefore, in this report, we explore the impact of a broader range of surfactants, oils and proteins on the expansion of epithelial cells, HaCaT cells and primary keratinocytes (HPKs), as well as bone marrow-derived mesenchymal stem cells (MSCs). We draw correlations between cell expansion at corresponding interfaces (relative to culture at the surface of tissue culture plastic, TPS) and associated interfacial mechanical properties. Specifically, we identify interfacial viscoelasticity as an important parameter correlating with cell expansion at liquid interfaces and develop methodologies to characterise this parameter at the micro- and macro-scale. Finally, we investigate the nanoscale architecture of protein nanoshseets via *in situ* neutron reflectometry and transmission electron microscopy and draw correlations between their observed multi length scale behaviours, and their ability to sustain stem cell expansion, retention of phenotype and cell sheet formation.

2. Results

2.1. Impact of surfactant chemistry on BSA nanosheet interfacial mechanics and HaCaT cell proliferation at liquid-liquid interfaces

The introduction of surfactant molecules such as pentafluorobenzoyl chloride has a striking impact on epithelial cell expansion at liquid interfaces [13,16]. To explore more broadly the role of surfactant chemistry on this phenomenon, the expansion of HaCaT cells (an epidermal cell line) was quantified at the surface of fluorinated oil interfaces supplemented with anionic (perfluorodecanoic acid, DecAc) and cationic (1H,1H-perfluorooctylamine, OctAm) surfactants, neutral perfluoro alkanes (1H,1H,2H,2H-perfluoro-1-decanol, DecOH and 1H,1H,2H-perfluoro-1-decene, DecEne) or reactive tensioactive molecules (sebacoyl chloride, SBCl; octanoyl chloride, OctCl; 2,3,4,5,6-pentafluorobenzoyl chloride, PFBCl; pentadecafluorooctanoyl chloride, PFOctCl), over a broad range of concentrations (Fig. 1A and B). In combination to bovine serum albumin (BSA), reactive surfactants were found to promote cell expansion to levels comparable to those observed for traditional 2D culture plastic (TPS), with SBCl and PFBCl enabling the formation of large spread colonies at the surface of oil interfaces. In contrast, non-reactive surfactants and neutral perfluoroalkyls led to the formation of small rounded cell clusters at best (see Supplementary Fig. S1).

As protein nanosheet mechanics was previously proposed to play an important role in enabling cell adhesion and colony formation [13], the impact of co-assembly of proteins and surfactants on interfacial mechanics was next examined. As elastic interfacial mechanics, normal to the plane of the interface, is not sufficiently sensitively quantified by AFM indentation due to overlapping contributions from surface tension and probe-interface coulombic interactions [13,20], we characterised liquid-liquid interfaces by interfacial rheology. This enables to isolate interfacial shear components, independent of changes in surface areas and associated mechanical contributions.

Upon introduction of bovine serum albumin, we observed a sharp

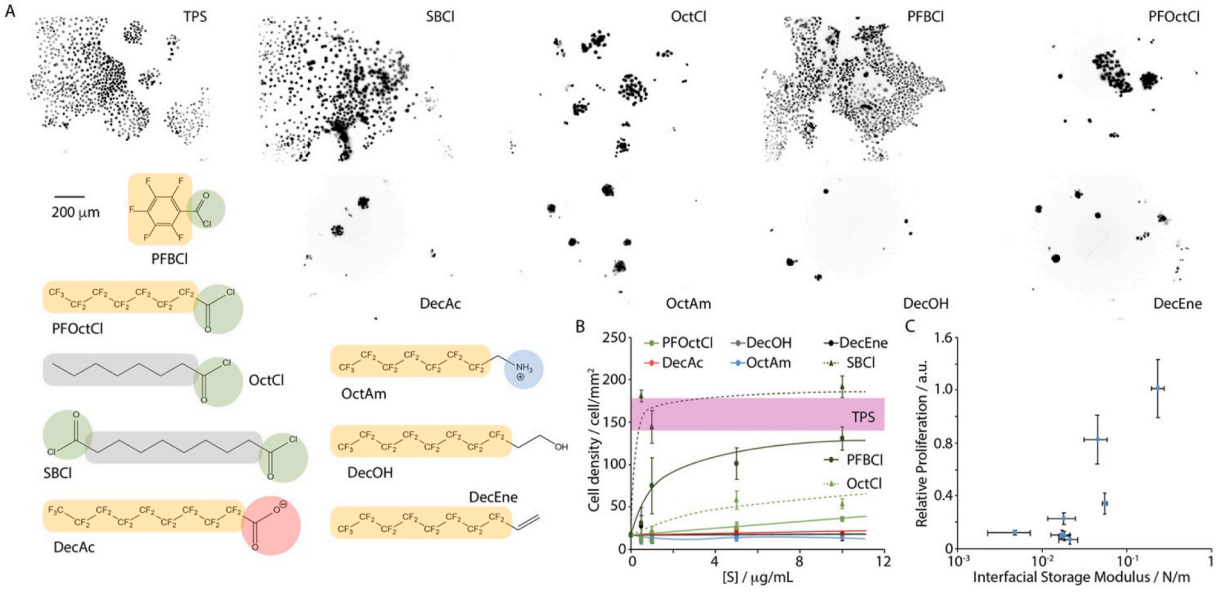

Fig. 1. Impact of surfactant chemistry and BSA nanosheet interfacial mechanics on cell expansion at liquid interfaces. A) HaCaT colonies formed at fluorinated oil interfaces (Novec 7500) containing different surfactants (sebacoyl chloride, SBCl; octanoyl chloride, OctCl; 2,3,4,5,6-pentafluorobenzoyl chloride, PFBCl; pentadecafluorooctanoyl chloride, PFOctCl; perfluorodecanoic acid, DecAc; 1H,1H-perfluorooctylamine, OctAm; 1H,1H,2H,2H-Perfluoro-1-decanol, DecOH and 1H,1H,2H-perfluoro-1-decene, DecEne; all at [S] = 10 µg/mL). The BSA concentration (in all conditions) was kept constant at 1 mg/mL. The Images are nuclear staining (Hoechst). B) Corresponding HaCaT cell densities at different surfactant concentrations (the error range of tissue culture polystyrene, TPS, is indicated as a purple area). C) Correlation between relative proliferation of cells (densities at corresponding oil interfaces relative to TPS, at day 7) with interfacial storage moduli (quantified from frequency sweeps in interfacial rheology experiments, at displacement of 1.0 10^{-3} rad and frequency of 0.1 Hz). Error bars are s.e.m.; n = 3. (For interpretation of the references to colour in this figure legend, the reader is referred to the Web version of this article.)

increase in interfacial storage and loss moduli, reaching plateaus after 15 min, although further maturation continued in some cases (Supplementary Fig. S2). In addition, whereas interfaces displayed significant frequency-dependant profiles and low interfacial moduli (below 10 mN/m) prior to protein adsorption, protein-stabilised interfaces displayed only slight frequency modulated mechanics (Supplementary Fig. S3). We noted that interfacial moduli were relatively high to start with in the case of non-fluorinated surfactants (with interfacial storage moduli significantly higher than the loss moduli, Supplementary Fig. S2), possibly due to phase separation at the interface between the fluorinated oil and aqueous phase, although this was not further explored. However, despite such initial high shear modulus, the storage modulus of SBCl and OctCl interfaces did increase upon adsorption of albumin. In contrast, in the case of fluorinated surfactants, whilst interfacial loss moduli were comparable to storage moduli prior to protein adsorption, the storage moduli of BSA nanosheet stabilised interfaces systematically increased significantly above loss moduli (Supplementary Fig. S2). These behaviours were particularly striking in the case of reactive acyl chloride surfactants. In contrast, charged surfactants and neutral perfluoroalkyls had a modest impact on the frequency dependency of BSA nanosheets. Anionic DecAc had little impact on BSA nanosheet mechanics (Supplementary Fig. S2), despite a higher interfacial modulus prior to protein adsorption. Cationic OctAm increased the interfacial mechanics of resulting nanosheets slightly. We note that all surfactants enabled the stabilisation of emulsions by BSA (Supplementary Fig. S4). The formation of nanosheets was clearly observed in all cases by scanning electron microscopy, as emulsions generated from corresponding formulations and dried after deposition on silicon substrates all displayed wrinkled morphologies (Supplementary Fig. S5).

We next set out to correlate the impact of interfacial mechanics on cell expansion. We plotted relative HaCaT cell expansion (compared to TPS controls) against interfacial storage (Fig. 1C). Although interfaces displaying low interfacial storage moduli (<20 mN/m) did not support cell proliferation, at higher interfacial moduli we generally observed an increase in colony formation and relative HaCaT proliferation. Interfaces promoting the highest HaCaT proliferation (to comparable levels to that of HaCaT proliferation on TPS) were associated with high interfacial shear moduli and corresponded to nanosheets formed in the presence of reactive acyl chloride surfactants (note that not all reactive surfactants performed equally well at promoting cell expansion; See Supplementary Table S1 for details). Hence surfactant reactivity and chemical coupling to BSA nanosheets is associated with increased interfacial shear modulus and cell proliferation. However, it is not completely clear how the chemical structure of surfactants impacted on interfacial mechanics and cell proliferation. Hence, whilst it could indeed be expected that difunctional surfactants such as SBCl can covalently crosslink nanosheets and that aromatic surfactants such as PFBCl may provide stronger physical crosslinks than corresponding aliphatic molecules, the aliphatic OctCl led to stronger interfaces than the fluorinated PFOctCl. Varying reactivities, detailed interactions and alteration of the protein nanosheet morphology, as well as altered interactions with further biomacromolecules that may foul the surface of nanosheets, may contribute to variations observed both in nanosheet mechanics and cell expansion potential between the reactive surfactants studied.

2.2. Impact of surfactant chemistry on poly(L-lysine) nanosheet interfacial mechanics and stem cell proliferation at liquid-liquid interfaces

As BSA does not sustain the adhesion of a broad range of cells, we next investigated the impact of interface composition (oil type, surfactant chemistry) on the proliferation of primary human keratinocytes (responsible for the self-renewal of the interfollicular epidermis) and mesenchymal stem cells (MSCs, bone marrow derived) at oil interfaces stabilised with poly (L-lysine) (PLL). Indeed, PLL is a protein routinely used to coat glass surfaces and other substrates, to promote the adsorption of extra-cellular matrix (ECM) proteins, such as fibronectin or laminin. Cell adhesion was investigated on Novec 7500 fluorinated oil and silicone (PDMS, 10 cSt) oils to broaden the range of interface chemistry examined, however we specifically focused on reactive surfactants, considering the impact coupling had on BSA nanosheet mechanics.

Keratinocytes and MSCs were found to proliferate at the surface of fluorinated and silicone oils, stabilised by PLL nanosheets in the presence of reactive surfactants, to comparable levels observed on tissue culture plastic (Fig. 2A and B and Supplementary Figs. S6–7). Surprisingly, in contrast to results observed with BSA nanosheets [13], within the same range of concentrations tested with HaCaT cells (1–10 μg/mL), PFBCl did not support cell proliferation at higher concentrations to the same extent. To examine how interfacial mechanics correlated with stem cell proliferation, we determined the interfacial shear moduli of corresponding interfaces and correlated these measurements with relative stem cell expansions (Fig. 2C and Supplementary Table S2). This comparison showed no correlation, with a high scatter of data at both high and low interfacial moduli.

Upon introduction of PLL within the aqueous phase, the interfacial modulus of corresponding interfaces (with Novec 7500) raised rapidly, although it reached a plateau more slowly than that of albumin nanosheets (Fig. 2D; typically after >2000 s following injection in the case of PLL, compared <2000 s in the case of BSA interfaces, see Supplementary Fig. S2). The plateau interfacial storage modulus was significantly affected by the concentration of surfactant used, reaching >1 N/m at 10 μg/mL PFBCl concentrations, 2 orders of magnitude above values observed for the assembly of BSA nanosheets in comparable conditions (except for the pH that was 10.5; compare data in Figs. 2D and 1C, and gathered in Supplementary Tables S1 and S2). This was also found to be the case at silicone oil interfaces, with heptadecanoyl chloride/sebacoyl chloride surfactant mixtures (this was selected on the basis of improved emulsion stability, see Supplementary Fig. S8). The reaction of acyl chloride surfactants with lysine-rich macromolecules such as PLL is therefore proposed to result in particularly stiff interfaces. Indeed, this hypothesis was further confirmed by studying the formation of lysosyme nanosheets at Novec 7500 and silicone oil interfaces, in the presence of reactive surfactants (Supplementary Fig. S9). The high lysine content of lysosyme, although lower than that of PLL, but higher than that of BSA, resulted in relatively stiff nanosheets, further highlighting the role of lysine residues in mediating nanosheet assembly and regulating mechanics. This is consistent with the higher reactivity of amines (e.g. from lysine residues) with acyl chlorides compared to alcohols (e.g. from serine residues).

Surprisingly, although all PLL nanosheets assembled displayed significantly higher moduli compared to BSA nanosheets generated in the presence of the same surfactant (and concentration), those formed at the highest PFBCl concentration (10 μg/mL) did not support the growth of MSCs and HPKs (Fig. 2C and Supplementary Table S2). This was despite applying the same fibronectin deposition protocol to all PLL interfaces. The absence of correlation between interfacial shear storage modulus and stem cell proliferation, in the case of PLL nanosheets was therefore surprising and suggested that other mechanical properties of protein nanosheets may contribute to regulate cell adhesion and mechanosensing at liquid interfaces.

2.3. Impact of surfactant chemistry on nanosheet viscoelasticity and cell proliferation

Although interfacial moduli did not correlate with relative cell expansion at liquid interfaces, we found that associated tan(δ) correlated better (Supplementary Fig. S10), with expansion indices above 0.5 at tan(δ) measured below 0.2 (Supplementary Tables S1 and S2). This suggested that viscous interfaces may not support cell expansion as well as elastic interfaces. Indeed, viscoelastic materials have been found to significantly impact cell adhesion and phenotype [21–24]. In order to

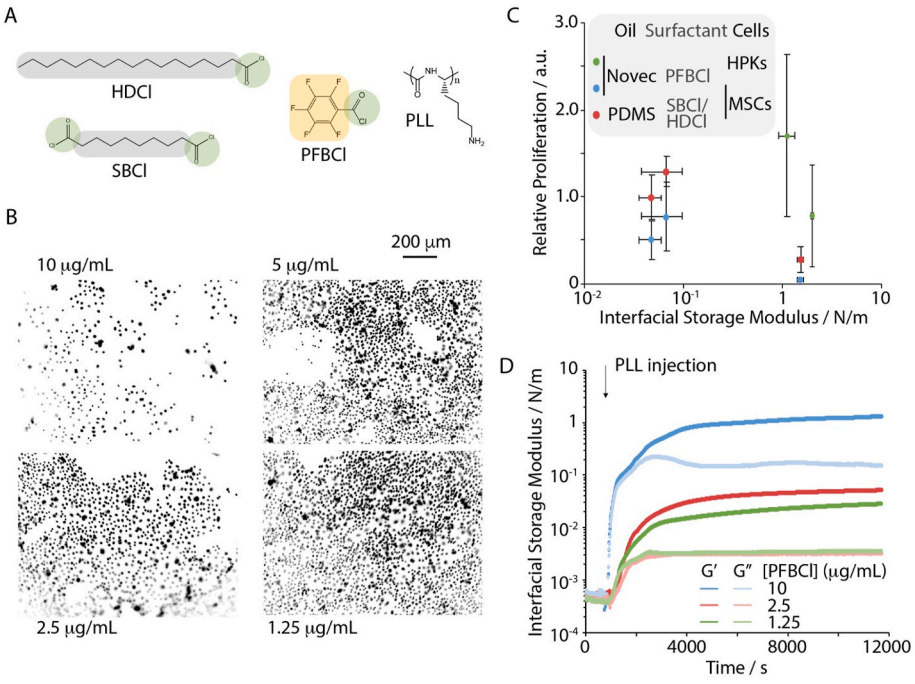

Fig. 2. Impact of surfactant chemistry, oil type and PLL nanosheet interfacial mechanics on cell expansion at liquid interfaces. A) Chemical structure of the surfactants used and poly (L-lysine) (PLL). HDCl is hexadecanoyl chloride; SBCl is sebacoyl chloride; PFBCl is pentafluorobenzoyl chloride. B) Images of nuclear stainings (Hoechst) of keratinocytes cultured at PFBCl/PLL interfaces on Novec 7500 (PLL, 100 μg/mL; PFBCl, 1.25, 2.5, 5 and 10 μg/mL), coated with fibronectin (10 μg/mL). C) Correlation between relative proliferation of cells (densities at corresponding oil interfaces relative to TPS, at day 7) with interfacial storage moduli. Green, HPKs cultured on Novec 7500 (PLL with PFBCl at different concentrations in the range of 1.25–10 μg/mL). Blue, MSCs cultured on Novec 7500 (PLL with PFBCl at different concentrations in the range of 1.25–10 μg/mL). Red, MSCs cultured on liquid silicone (PDMS, 10 cSt, PLL with HDCl/SBCl at 10 and 100 μg/mL). D) Representative time sweeps (frequency, 0.1 Hz; strain, 1%) profiling changes in interfacial shear storage and loss moduli during the assembly of PLL (100 μg/mL) at Novec 7500 interfaces, in the presence of PFBCl at different concentrations, In PBS (pH adjusted to 10.5). Error bars are s.e.m.; n = 3. (For interpretation of the references to colour in this figure legend, the reader is referred to the Web version of this article.)

quantify the interfacial viscoelasticity of protein nanosheets assembled at liquid-liquid interfaces, we developed interfacial stress relaxation protocols, based on shear strain of a du Noüy ring at corresponding interfaces (Supplementary Fig. S11). Normalised stress relaxation profiles were fitted with a double exponential decay, in order to extract relaxation parameters as well as associated relaxation amplitudes and elastic components. The level of elasticity of protein nanosheet-stabilised interfaces was quantified via the determination of the elastic component (residual normalised stress after relaxation, σ_r, expressed in %; see methods).

The elasticity of BSA nanosheets was quantified first (Fig. 3A and Supplementary Fig. S12). Stress retentions varied between 10 and 90%, depending on the nature of the surfactant used. High interfacial elasticity was typically observed in the presence of reactive acyl chloride surfactants, whereas in the absence of any surfactant (but in the presence of BSA) interfaces displayed the lowest degree of elasticity (Supplementary Table S1). This suggests that BSA molecules adsorb at interfaces, forming poorly integrated and crosslinked networks, but that the coupling of hydrophobic residues, through reactive surfactants, results in significant level of physical crosslinking. It may also be possible that the increased hydrophobicity associated with resulting nanosheets results in further protein adsorption and more extensive coverage of the liquid-liquid interface.

Correlations between σ_r and relative HaCaT expansion (Fig. 3B) were in excellent agreement with correlations made between the interfacial storage modulus and cell expansion (Fig. 1C), reflecting the increased elasticity observed for the stiffest BSA nanosheets. Similarly, the elasticity of PLL nanosheets displayed improved correlation with stem cell expansion at liquid interfaces (Fig. 3C). Indeed, at low stress retention (59%), keratinocytes and MSC proliferation was restricted, compared to interfaces displaying higher degrees of elasticity (σ_r up to 87%). Pulling all data together further confirmed the improved correlation observed between interfacial elasticity and cell proliferation, compared to that of storage or loss moduli (Supplementary Fig. S13). Above a threshold of stress retention of 60%, cell proliferation was systematically comparable or higher to that observed for the same cell type on tissue culture plastic. This is consistent with the importance of elasticity to resist cell-mediated traction forces and trigger the reinforcement of cell adhesions [23]. Overall, our data suggest that non-reactive co-surfactants do not contribute significantly to the crosslinking of protein networks, whereas covalent coupling of reactive co-surfactants enables the formation of physical (in the case of PFBCl, PFOctCl, heptadecanoyl chloride (HDCl) and OctCl) and covalent crosslinks (i.e. with SBCl), and this associated increase in elasticity contributes to regulate cell proliferation.

Interestingly, we did not observe clear correlations between cell expansion at liquid interfaces, for the different systems studied, and relaxation times extracted from stress relaxation experiments (Supplementary Fig. S14). This observation contrasts with such correlations made in the case of cell phenotype at the surface or within hydrogels [22]. This may indicate that key mechanical parameters regulating cell expansion at liquid interfaces are not only the time scale at which relaxation processes are taking place, but also their magnitude, and associated σ_r. We also note that in viscoelastic 3D hydrogels, faster relaxation is required to enable cell protrusion and matrix physical remodelling. This is a distinct scenario and context to the present 2D interface. Therefore the amount of energy that can be stored in corresponding networks, upon cell-mediated deformation, rather than the kinetics of associated processes alone, may regulate cell phenotype.

We also observed that the ζ-potentials of PLL nanosheets generated in the presence of different PFBCl concentrations, or those of BSA nanosheets generated in the presence of different co-surfactants were comparable (Supplementary Fig. S15). Therefore, variations in electrostatic potential, which may result in changes in cell adhesive protein adsorption, were not observed. In turn, we observed comparable surface densities (quantified via fluorescence microscopy) of PLL and BSA, in the presence of different concentrations of PFBCl and different co-surfactants, respectively (Supplementary Fig. S16). In addition, fibronectin adsorption to PLL nanosheets formed in the presence of different PFBCl concentrations was comparable and protein adsorption from foetal bovine serum (FBS) to BSA nanosheets formed in the presence of different co-surfactants was also comparable (Supplementary Fig. S16). Only BSA nanosheets assembled in the presence of non-fluorinated co-surfactants SBCl and OctCl displayed reduced FBS protein adsorption, although it is not clear whether this correspond to a reduction in cell-adhesive protein adsorption (see Supplementary Discussion on this point).

Surprisingly, in the case of PLL nanosheets, σ_r did not correlate with storage moduli. Hence, PLL nanosheets assembled at Novec 7500

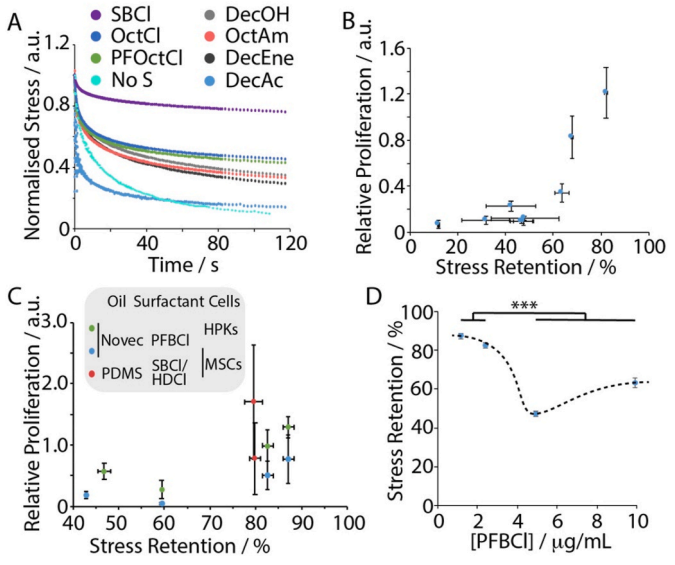

Fig. 3. Interfacial viscoelasticity regulates cell expansion at liquid interfaces. A) Stress relaxation of interfaces between fluorinated oil (Novec 7500) and PBS, in the presence of different surfactants (10 µg/mL) and BSA (1 mg/mL). "No S" corresponds to the stress relaxation profile of BSA-stabilised interfaces without any surfactant. B) Correlation between relative proliferation of HaCaT cells (densities at corresponding oil interfaces relative to TPS, at day 7) spreading on BSA nanosheets formed in the presence of different surfactants (as in Fig. 1) with interfacial elasticity (quantified from stress relaxation experiments, as the stress retention, corresponding to the elastic component of interfaces). C) Correlation between relative proliferation of cells (densities at corresponding oil interfaces relative to TPS, at day 7) with interfacial elasticity (quantified as the stress retention). Green, HPKs cultured on Novec 7500 (PLL with PFBCl at different concentrations in the range of 1.25–10 µg/mL). Blue, MSCs cultured on Novec 7500 (PLL with PFBCl at different concentrations in the range of 1.25–10 µg/mL). Red, MSCs cultured on liquid silicone (PDMS, 10 cSt, PLL with HDCl/SBCl at 10 and 100 µg/mL). D) Stress retention associated with PLL-assembled fluorinated oil interfaces (Novec 7500, PLL 100 µg/mL, pH 10.5) in the presence of PFBCl at different concentrations. Error bars are s.e.m.; n = 3. (For interpretation of the references to colour in this figure legend, the reader is referred to the Web version of this article.)

interfaces in the presence of PFBCl displayed reduced elasticity at 5 and 10 µg/mL, compared to 1.25 and 2.5 µg/mL (Fig. 3D). Whereas the interfacial modulus of these nanosheets increased with increasing PFBCl concentrations (Fig. 2D and Supplementary d S2), it led to a reduction in σ_r and cell proliferation (Fig. 3D and Supplementary Figs. S6–7).

2.4. Origin of variations in interfacial viscoelasticity observed in PLL nanosheets

In order to investigate the origin of such phenomenon, we imaged the formation of tagged PLL nanosheets (Fig. 4A). Surprisingly, even at very early time points (15 s), significant levels of PLL adsorption was found to occur and fluorescence intensity did not increase at later time points. However, at early time points, PLL assemblies were associated with flow patterns that suggested a relatively fluid interface. This is in agreement with the evolution of the interfacial shear moduli of PLL nanosheet-stabilised interfaces as a function of assembly time (Fig. 2D). Indeed, both storage and loss moduli were found to rapidly increase upon injection of PLL solutions, yet remained comparable in magnitude at early time points. The tan(δ) of corresponding interfaces decreased slightly upon protein injection (at [PFBCl] = 10 µg/mL, from >1.0 to c.a. 0.8, as moduli started to increase), but remained relatively constant during the initial phase of nanosheet maturation (Supplementary Fig. S17). 300–900 s after PLL injection, depending on the concentration of PFBCl, the tan(δ) started to decrease slowly to reach plateaus in the range of 0.06–0.12, depending on the condition. This was associated with a disappearance of flow patterns and the establishment of homogenous protein nanosheets (after 180 s, at the mm scale), which subsequently started to fragment into large domains (several hundreds of µm across) as a result of deformations induced by shear flow (during sample handling). Therefore our interfacial rheology and fluorescence microscopy data suggest the occurrence of molecular jamming of initially fluid PLL assemblies, whilst their rigidity (interfacial storage modulus) continues to increase. Ultimately, this leads to brittle fracture of nanosheets, as a result of shear deformation and their relaxation in macroscale interfacial rheology experiments.

These observations led us to propose that the viscoelastic profile of protein nanosheets could vary significantly at the macroscale (probed by our interfacial rheology set up) and at the nano-to micro-scale. To test this hypothesis, we developed an interfacial microrheology assay, based on creep experiments in which magnetic microparticles exert shear forces on protein nanosheets under stress control operated by magnetic tweezers (Fig. 4B). The creep displacement profile is then analysed in order to extract corresponding creep compliances that can be plotted against time and fitted with a 6-elements Burger's model (Fig. 4C and Supplementary Fig. S18; see Methods). Due to the need for strong adhesion between nanosheets and the magnetic probe used for these experiments, we were only able to characterise PLL nanosheets using this assay and focused on a comparison of the microscale rheological properties of nanosheets generated at low (1.25 µg/mL) and high (10 µg/mL) PFBCl concentrations. Microrheology profiles of PLL nanosheets co-assembled with the co-surfactant PFBCl indicated significant levels of elasticity (G_0) at high PFBCl concentrations, and reduced levels of viscosity (G_1), with higher levels of stress recovery, compared to nanosheets generated at low PFBCl concentrations (Fig. 4C and D and Supplementary Fig. S18). Therefore, microrheology experiments confirm that, at the nano-to microscale, rigid PLL nanosheets generated at 10 µg/mL PFBCl display rigid elastic mechanical profiles and that the viscoelastic profiles observed via interfacial rheology arise from fractured domain rearrangement in response to shear deformation.

2.5. Nanoscale architecture of viscoelastic protein nanosheets

In order to identify structural parameters regulating protein nanosheet viscoelasticity, the nanoscale architecture of these assemblies was next examined. We focused on a subset of four nanosheets displaying very distinct interfacial mechanics: 1. BSA nanosheets displaying moderate interfacial storage moduli and low elasticity; 2. BSA nanosheets formed in the presence of acyl chloride co-surfactant (PFBCl or HDCl, 10 µg/mL) and displaying moderate interfacial storage moduli and high elasticity; 3. PLL nanosheets formed at low co-surfactant concentrations (1.25 mg/mL) or pH (7.4) and displaying moderate moduli and high elasticity; 4. PLL nanosheets formed at high co-surfactant concentrations (10 µg/mL) and pH (10.5) and displaying high moduli and moderate elasticity due to a brittle character.

Polarised optical microscopy was first used to examine whether molecular organisation and ordering could be observed. Although Novec 7500 microdroplets stabilised by BSA alone showed no evidence of polarisation, comparable to droplets stabilised by Tween 20 (used as reference here as not expected to display structure), droplets stabilised by BSA/PFBCl or PLL/PFBCl nanosheets displayed circumferential hallos indicative of structural polarisation (Fig. 5A and Supplementary Fig. S19). The halo had a homogenous intensity and colour for BSA/PFBCl and PLL nanosheet-stabilised droplets at a concentration of PFBCl of 10 µg/mL, but appeared weaker and fragmented at a concentration of 1.25 µg/mL (Fig. 5A). Similarly, whereas no hallo was observed for BSA-stabilised hexadecane microdroplets, a diffuse hallo was observed for BSA-stabilised droplets in the presence of 10 µg/mL heptadecanoyl chloride (HDCl; Supplementary Fig. S19). These hallos are reminiscent of the structures observed by polarised optical microscopy at early

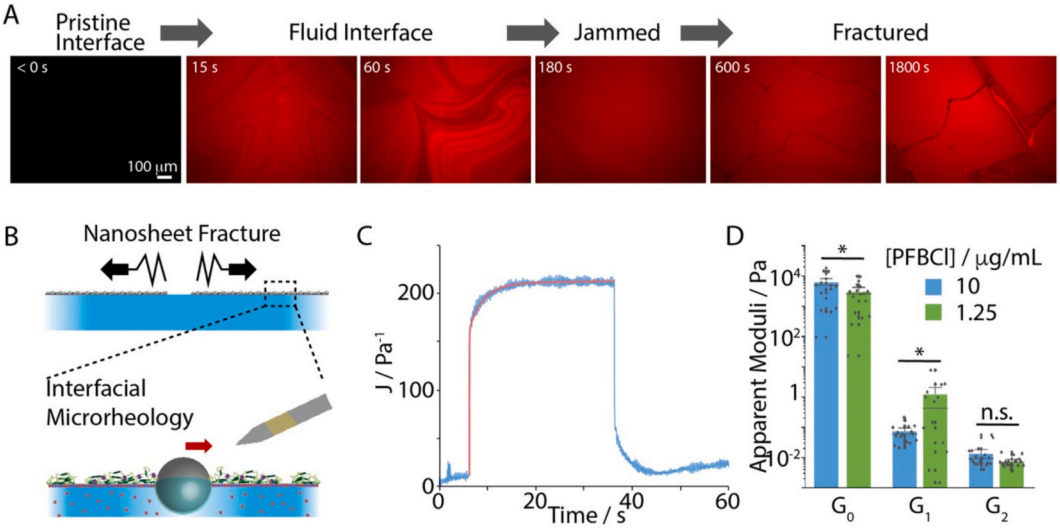

Fig. 4. Interfacial viscoelasticity at the micro- and macroscale do not correlate. A) Tagged PLL assembling at fluorinated oil interfaces (different time points, Novec 7500, PFBCl 10 µg/mL, pH 10.5). To stop the assembly process, the pH of solutions was reduced below 5.0 by adding a drop of 1 M HCl. B) Schematic representation of a protein nanosheet fragmenting at the macroscale and characterised by interfacial microrheology at the microscale. C) Representative creep-recovery traces obtained using magnetic tweezers at a PLL-stabilised Novec 7500 interface with PBS (PLL, 100 µg/mL; PFBCl, 10 µg/mL; pH 10.5). D) Shear moduli extracted from creep measurements (6-element Burger's model; blue, 10 µg/mL; green, 1.25 µg/mL). Error bars are s.e.m.; n = 3. (For interpretation of the references to colour in this figure legend, the reader is referred to the Web version of this article.)

stages of droplet deformation driven by intermediate rotator phases upon cooling close to freezing point in the presence of appropriate surfactants (although arising from very different phenomena) [25] and indicate a degree of organisation and structure in co-surfactant-stabilised protein nanosheets.

To gain further insight into the nanoscale architecture of protein nanosheets, we carried out neutron reflectometry experiments. In order to study the structure of pristine nanosheets assembled at liquid-liquid interfaces, we studied interfaces formed with a thin layer of hexadecane contrast matched to silicon, generated via the spin-freeze-thaw method [26]. Other liquids used in other section of our work (Novec 7500 and silicone oils) could not be studied via neutron reflectometry as their freezing point was too low to enable us to transfer thin films to the liquid cells positioned into the neutron beam set up. BSA nanosheets, with and without HDCl, displayed near identical reflectivity profiles that could be fitted to bilayer morphologies with comparable scattering length density profiles (Fig. 5B and C). These bilayers are characterised by a first layer in contact with the oil phase, relatively thick (7.2–7.7 nm) and a high protein density (75 wt%), and a shallower hydrophilic second layer (3.3–3.6 nm) displaying significant water content (78 wt %). This is in line with the structure of BSA monolayers generated in the absence of HDCl at lower pH [27]. Therefore, the presence of HDCl had a very modest impact on the architecture of BSA nanosheets.

In contrast, the architecture of PLL nanosheets was found to be significantly affected by the density of co-surfactants, although reflectivity profiles could also be fitted by bilayer models (Fig. 5B and C). At high pH, when significant coupling of co-surfactant to PLL is observed [10], the thickness of the oleophilic layer was only 3.6 nm, with a moderate protein content (60 wt%). The thickness of the hydrophilic layer was also thinner, compared to BSA nanosheets, with a thickness of 1.9 nm and a water content of 87 wt%. At lower pH, when coupling of co-surfactant is restricted due to protonation of lysine residues, the thickness of the oleophilic layer was reduced to 3.0 nm, with only 58 wt % of protein content, whereas the hydrophilic layer extended to 3.3 nm, with a water content of 82 wt%. Such reduction in protein content in the oleophilic layer, together with a reduced thickness, is indicative of the formation of a quasi-2D network of protein domains, separated by low protein content domains (Fig. 5D, top). In contrast, BSA nanosheets, are proposed to display more homogenous oleophilic phases, with a reduced degree of structure.

We note that nanosheets formed at the surface of different oils and in the presence of different co-surfactants are expected to display different morphologies and associated physico-chemical and mechanical properties. Hence the nanosheet morphologies characterised at hexadecane interfaces in the presence of HDCl may not necessarily reflect the exact architecture of nanosheets formed at Novec 7500 interfaces. Extrapolation of our result from one system to another should therefore be cautious. However, we observed comparable nanosheet formation (from the monitoring of interfacial storage moduli in time sweep experiments) on different oil interfaces studied in the present work (Novec 7500, hexadecane and PDMS) and frequency sweeps and stress relaxation profiles indicated comparable viscoelastic properties (Supplementary Fig. S20). Therefore, we propose that, although nanosheets formed on one interface may differ in chemistry and morphology slightly, providing similar types of proteins and surfactants are used, compatible with the oil system investigated, data obtained for one oil may provide some insight into the behaviour of nanosheets formed on other oils. Neutron reflectometry systems that would allow direct measurements to be carried out *in situ* at relevant oil-water interfaces would certainly help lifting the approximations made in these extrapolations, but such platforms are currently not available.

To directly visualise the occurrence of domains in protein nanosheets, we used transmission electron microscopy. Nanosheets were assembled at Novec 7500-deionised water interfaces and transferred to TEM grids via Langmuir-Blodgett deposition, using a purpose-built trough for liquid-liquid interfaces. The four BSA and PLL nanosheets imaged were clearly amorphous, with relatively large intact areas, although gaps were apparent, possibly due to nanosheet rupture occurring during transfer and sample dehydration (Fig. 5E). None of the protein nanosheets examined displayed any sign of crystallinity or ordered architecture. However, high resolution images clearly indicated the occurrence of small (<10 nm) disordered domains of increased density (appearing dark). These domains appeared larger yet isolated in BSA-PFBCl nanosheets compared to BSA nanosheets. We note that these domains are reminiscent of β-lactoglobulin domains imaged at air-liquid interfaces by AFM, but displaying less homogenous morphologies [28], possibly highlighting differences in assembly and nanosheet formation at liquid-liquid, compared to air-liquid interfaces. PLL nanosheets

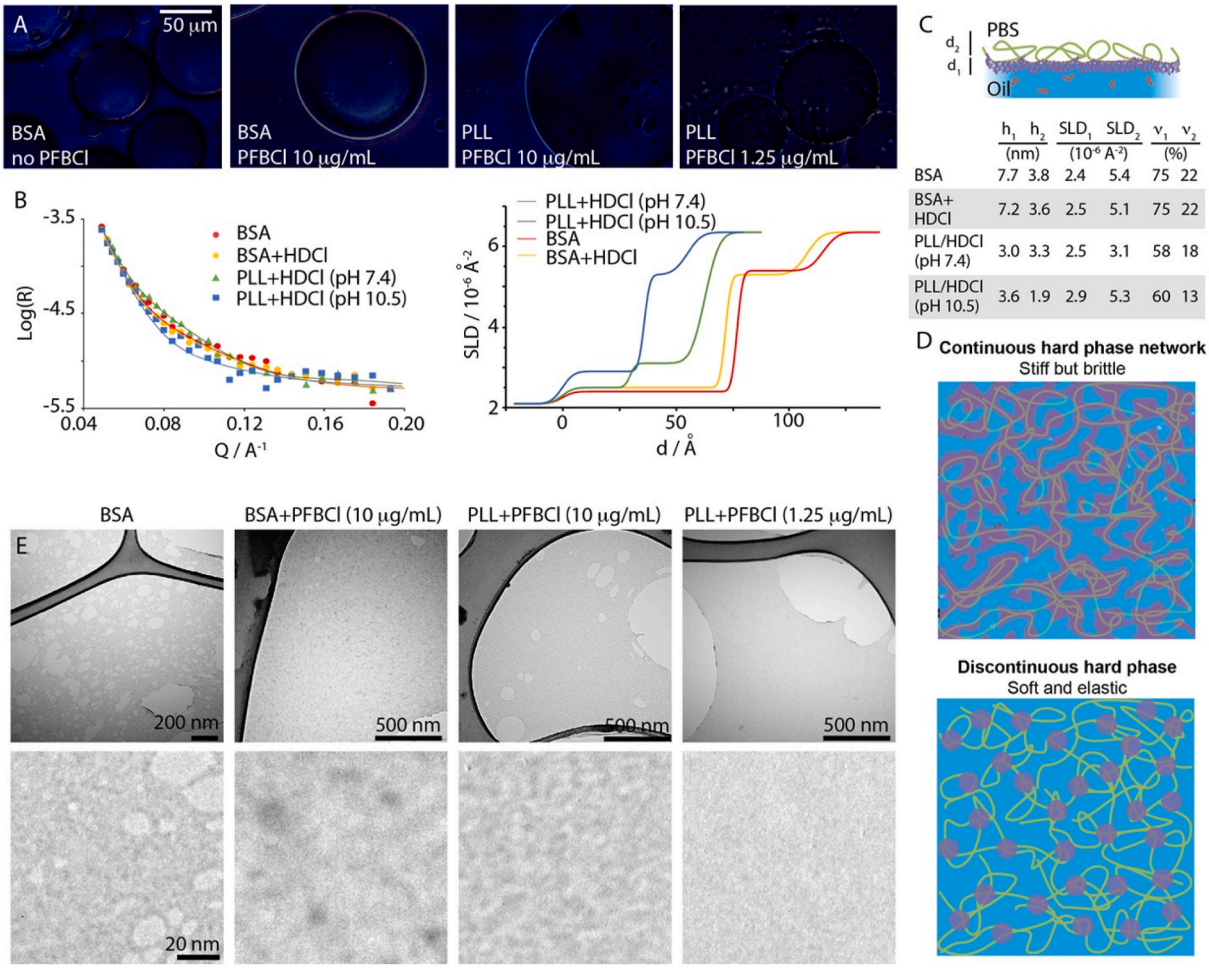

	h_1 (nm)	h_2 (nm)	SLD_1 (10^{-6} Å^{-2})	SLD_2 (10^{-6} Å^{-2})	ν_1 (%)	ν_2 (%)
BSA	7.7	3.8	2.4	5.4	75	22
BSA+ HDCl	7.2	3.6	2.5	5.1	75	22
PLL/HDCl (pH 7.4)	3.0	3.3	2.5	3.1	58	18
PLL/HDCl (pH 10.5)	3.6	1.9	2.9	5.3	60	13

Fig. 5. The Nanoscale morphology of protein nanosheets correlates with changes in visco-elastic properties. A) Representative polarised optical microscopy images of Novec 7500 emulsions stabilised with different proteins (1 mg/mL BSA or 0.1 mg/mL PLL) and PFBCl (concentrations indicated on images). B) Reflectivity (R) plotted as a function of scattering wave vector (Q) and associated Scattering Length Density (SLD) profiles of BSA (1 mg/mL), BSA (1 mg/mL)/HDCl (10 μg/mL), PLL (100 μg/mL, pH 7.4)/HDCl (10 μg/mL) and PLL (100 μg/mL, pH 10.5)/HDCl (10 μg/mL) nanosheets assembled at hexadecane/PBS interfaces. C) Summary of parameters extracted from the fits of neutron reflectometry data. D) Schematic representation of the proposed molecular assembly of protein network at oil−water interfaces. Hard phases are represented in purple. E) Representative TEM images of BSA and PLL nanosheets transferred via Langmuir-Blodgett deposition from fluorinated oil (Novec 7500)-water interfaces. BSA: alone or with PFBCl (10 μg/mL); PLL (100 μg/mL, pH 10.5) with PFBCl (10 or 1.25 μg/mL). (For interpretation of the references to colour in this figure legend, the reader is referred to the Web version of this article.)

assembled in the presence of PFBCl at 1.25 μg/mL appeared comparatively more uniform, with small disconnected granularity, whereas in the presence of PFBCl at 10 μg/mL, a network of interconnected domains could be observed. This network is proposed to arise from the increased degree of coupling with PFBCl, which was confirmed by X-ray photoelectron spectroscopy carried out on dried nanosheets (Supplementary Fig. S21), reaching 46.8 ± 6.5% functionalisation (10.6 ± 1.5% of F atom) at a concentration of PFBCl of 10 μg/mL.

Taken together, our data indicate that BSA nanosheets display a homogenous amorphous structure and that reactive co-surfactants such as PFBCl induce the occurrence of denser domains that act as effective physical crosslinks (Fig. 5E, bottom), leading to an increase in σ_r from 12 to 63%, without significant increase in the overall modulus of the nanosheet (2.2 fold, as would be expected from a simple rule of mixture of isolated hard phases dispersed within a soft matrix). In contrast, PLL nanosheets formed at 10 μg/mL PFBCl display a far more rigid behaviour (1.52 ± 0.12 N/m) compared to nanosheets formed at 1.25 μg/mL (67.7 ± 30.4 mN/m). Considering the thickness of PLL nanosheets measured *in situ* (3.0–3.6 nm), the mechanical properties of PLL nanosheets generated at high PFBCl concentrations correspond to a bulk Young's modulus of 1.5 GPa (assuming a Poisson ratio of 0.5). Such rigid behaviour can only be accounted for assuming a continuous oleophilic hard phase. However the relatively low PLL content in the oleophilic layer (60%, Fig. 5D) suggests a continuous network of hard phases separated by hydrophilic domains (Fig. 5D, top). The rigidity of this network is associated with a brittle character that leads to the formation of large domains and a reduction in the elastic character of the interface at the macroscale. At lower [PFBCl], the decrease of hard phases (19.9 ± 3.3% functionalisation) leads to the formation of discontinuous hard phases that contribute to physical crosslinking and the generation of more elastic (σ_r of 87%) yet softer nanosheets, comparable to those formed by BSA in the presence of PFBCl (Fig. 5D, bottom).

Therefore, quasi-2D protein nanosheets assembled at liquid-liquid interfaces are unique as, unlike other 2D or quasi-2D nanostructures studied to date often displaying a high degree of order and rigidity at the nanoscale, they extend to the meso and macroscale. Indeed, peptide and peptoid nanosheets can assemble at solid and liquid interfaces and display unique architectures and hierarchical structures [29,30]. However, although 2D nanomaterials can make excellent emulsion stabilisers [31], their assembly is typically restricted to the formation of micron size domains, limiting their application in platforms requiring long range interfacial shear elasticity. However, such control of architecture may be useful to fine-tune the properties of hard domains and their assembly within a soft interfacial matrix.

2.6. Impact of PLL nanosheet elasticity on stem cell adhesion and formation of stem cell sheets

To explore how the viscoelastic properties of protein nanosheets affected the adhesion of stem cells at the surface of liquid substrates, keratinocytes and MSCs were seeded at the surface of PLL-stabilised pinned droplets functionalised with fibronectin, and allowed to spread for 24 h prior to immunostaining and imaging. On all interfaces, cells were found to assemble focal adhesions sustaining the assembly of a well-structured actin cytoskeleton and stress fibres (Fig. 6A and B and Supplementary Fig. S22). Hence, within the range of viscoelastic properties achievable on these interfaces, cell adhesion and mechanosensing of corresponding interfaces was enabled. In fact, softer, yet more elastic nanosheets were found to increase keratinocyte spreading, similarly to the impact of the fluidity of cell adhesive ligands within supported lipid bilayers [23] and in agreement with the impact of hydrogel viscosity on cell adhesion, displaying a biphasic response to hydrogel stiffness and viscoelasticity, depending on ligand density [21,32]. The ability of cells to spread at liquid interfaces reinforced by elastic nanosheets is fully consistent with the accepted mechanism via which cells generate forces at planar interfaces. Indeed, traction forces and deformations arise from actin treadmilling parallel to the cell membrane [33] and actin stress fibre contraction transmitting tension to adhesions at angles lower than 15° with respect to the plane of the membrane and substrate [34]. In this respect, the data presented in this study, together with our previous results [13], the modest contribution of transverse forces and cell-mediated deformations expected at planar interfaces [35], and the important mechanical anisotropy associated with nanosheet-reinforced liquid interfaces [20], do not suggest a significant contribution of surface tension on the regulation of cell adhesion to corresponding interfaces.

Although, the reduction in macroscale elasticity observed in PLL nanosheets at high PFBCl concentrations did not prevent adhesion formation and cell spreading, it led to the fracture of nanosheets, either prior to cell seeding, during substrate functionalisation, or upon cell-mediated deformation of nanosheets. Even at low PFBCl concentrations, nanosheets were found to fracture, although they did not completely disrupt and prevent the formation of dense cell monolayers (Supplementary Figs. S23–24). Large gaps (sometimes several hundreds of micron across) can appear in between cell colonies that are completely devoid of any PLL nanosheets. In contrast, this behaviour was not observed on albumin nanosheets and cells formed homogenous colonies that completely covered the liquid surface. Analysis of resulting HPK monolayers indicated the formation of closely packed epithelial layers of comparable density to monolayers formed on functionalised glass substrates (Fig. 6C). In addition, these monolayers clearly featured

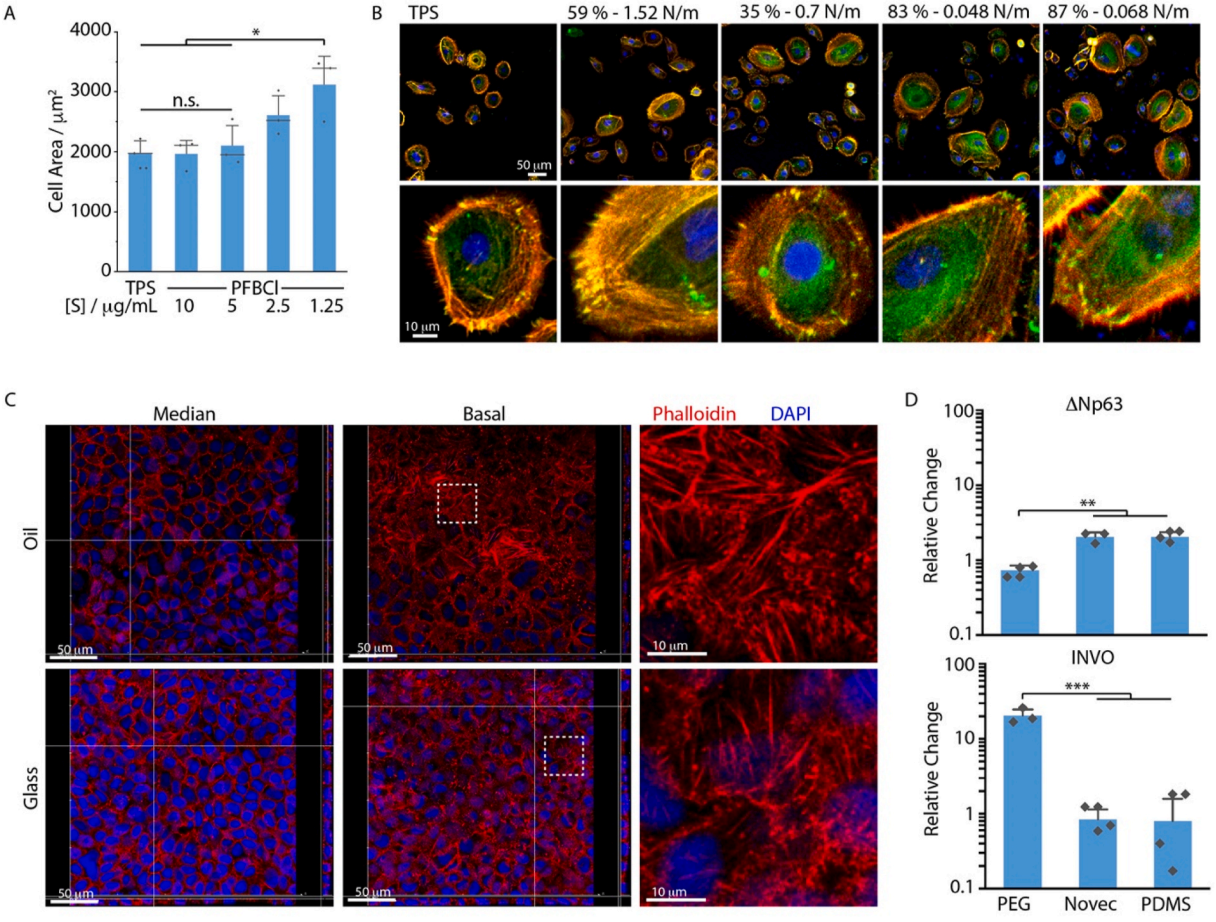

Fig. 6. Regulation of stem cell adhesion and expansion at liquid interfaces. A) Primary keratinocytes spreading (24 h) on fluorinated oil interfaces (Novec 7500, pH 10.5, PLL 100 µg/mL PFBCl at 10, 5, 2.5 and 1.25 µg/mL, fibronectin coated; compared to tissue culture polystyrene, TPS). Cell areas determined from actin staining (phalloidin). B) Corresponding confocal microscopy images (blue, DAPI; red, phalloidin; green, vinculin). C) HaCaT cell sheets generated on PLL coated glass and Novec 7500 interfaces (with fibronectin functionalisation). Top view of confocal z-stacks showing median and basal images (red, actin; blue, nuclei). D) Quantification of ΔNp63 and involucrin expression in HPKs cultured on: 1. PLL-PEG (100 µg/mL) coated substrate (FAD medium), 2. Novec 7500 oil (PLL 100 µg/mL, PFBCl 1.25 µg/mL, fibronectin 10 µg/mL, KSFM medium) and 3. Silicone oil (PDMS, 10 cSt, PLL 100 µg/mL, OctCl 50 µg/mL, fibronectin 10 µg/mL, KSFM medium). Quantification relative to cell cultured on TPS in FAD medium. Error bars are S.D.; n = 3. (For interpretation of the references to colour in this figure legend, the reader is referred to the Web version of this article.)

stress fibres at the basal interface, further confirming the mechanical engagement of these resulting dense cell colonies with the underlying substrate.

The phenotype of HPKs cultured at liquid-liquid interfaces was characterised at the transcription level, on fluorinated (Novec 7500) and silicone oil interfaces, and compared to cells cultured on TPS and PLL-PEG coated substrates (to induce cell rounding and differentiation). Phenotypes of cells growing at viscous interfaces were not investigated as cells did not proliferate for prolonged periods of times. Stem cell and proliferation markers ITGB1, DLL1, and MCSP [36,37] remained highly expressed in cells cultured at viscoelastic interfaces and ΔNp63 was even slightly upregulated (Fig. 6D and Supplementary Fig. S25). In addition, the expression of differentiation genes involucrin and filaggrin remained low, further confirming the absence of commitment to differentiation, in agreement with the impact of cell spreading on keratinocyte fate decision [18,38]. Hence, viscoelastic protein nanosheets not only enabled the proliferation of cells to high densities at the surface of liquids, comparable to those achieved on solid substrates, but also enabled to retain stem cell phenotypes and prevent differentiation, despite the softness of the liquid substrates used for such culture. This is in good agreement with the correlation often reported between stem cell phenotype and cell adhesion and morphology [36,39]. In addition to these observations, a more exhaustive characterisation of the long term phenotype of stem cells such as mesenchymal stem cells, upon culture at protein nanosheet-reinforced liquid interfaces, was also recently reported [40].

Our results demonstrate that amorphous nanosheets that are physically crosslinked by interactions with co-surfactant molecules display high levels of elasticity, despite softer interfacial shear mechanical properties, and support rapid adherent cell expansion whilst preserving their phenotypes. Together, these results indicate that nanosheets displaying modest interfacial moduli (in the range of 30–50 mN/m), but high elasticity, owing to the crosslinking (physical or covalent) of soft domains, are ideally suited for cell culture at liquid interfaces. The understanding of the mechanism via which the complex multiscale viscoelastic behaviour of protein nanosheets is determined by their nanoscale architecture will enable the more systematic engineering of such platforms for stem cell technologies and manufacturing. In addition, it remains most likely that a range of other physico-chemical parameters further modulate cell spreading, adhesion, proliferation and fate decision at nanosheet-stabilised liquid interfaces. Overall, our data suggests that interfacial viscoelasticity contributes to regulate adherent cell proliferation at liquid interfaces. Such understanding calls for the systematic design of liquid-liquid systems that enable the control of interfacial shear moduli and viscoelasticity, independently of each other. Such control is currently not possible with protein nanosheets identified to date. Protein nanosheets with controlled interfacial mechanics can then be applied to the design of emulsion-based bioreactors that will enable the simplification of processing of cell products, whilst enabling scale up and cost reduction.

Credit author statement

Dexu Kong: Data curation, Formal analysis, Investigation, Methodology, Writing – original draft, Writing – review & editing. Lihui Peng: Data curation, Formal analysis, Investigation, Methodology, Writing – original draft, Writing – review & editing. Minerva Bosch-Fortea: Data curation, Formal analysis, Investigation, Methodology. Alexandra Chrysanthou: Data curation, Formal analysis, Investigation, Methodology. Cardee V. J-M. Alexis: Data curation, Formal analysis. Carlos Matellan: Data curation, Formal analysis, Investigation, Methodology, Writing – original draft. Ali Zarbakhsh: Conceptualization, Data curation, Formal analysis, Investigation, Methodology, Writing – original draft. Giulia Mastroianni: Data curation, Formal analysis, Methodology. Armando del Rio Hernandez: Conceptualization, Formal analysis, Methodology, Writing – original draft. Julien E. Gautrot: Conceptualization, Formal analysis, Methodology, Writing – original draft, Writing – review & editing, Project administration, Resources.

Declaration of competing interest

The authors declare that they have no known competing financial interests or personal relationships that could have appeared to influence the work reported in this paper.

Acknowledgements

Funding for this work from the European Research Council (ProLiCell, 772462 and ProBioFac, 966740), the China Scholarship Council (studentship, 201708060335) and the Leverhulme Trust Foundation for financial support (RPG-2017-229, Grant 69241) is gratefully acknowledged. We thank Dr Stoyan Smoukov for help with polarise optical microscopy and Dr Richard Whiteley for help with XPS. We gratefully acknowledge the Science and Technology Facilities Council (STFC) for access to neutron beamtime at ISIS.

Appendix A. Supplementary data

Supplementary data to this article can be found online at https://doi.org/10.1016/j.biomaterials.2022.121494.

References

[1] A. Trounson, C. McDonald, Stem cell therapies in clinical trials: progress and challenges, Cell Stem Cell 17 (2015) 11–22.
[2] S.W. Lane, D.A. Williams, F.M. Watt, Modulating the stem cell niche for tissue regeneration, Nat. Biotechnol. 32 (2014) 795–803.
[3] H. Clevers, Modeling development and disease with organoids, Cell 165 (2016) 1586–1597.
[4] D.G. Phinney, M.F. Pittenger, Concise review: MSC-derived exosomes for cell-free therapy, Stem Cell. 35 (2017) 851–858.
[5] A. Aijaz, et al., Biomanufacturing for clinically advanced cell therapies, Nat. Biomed. Eng. 2 (2018) 362–376.
[6] F.F. dos Santos, P.Z. Andrade, C.L. da Silva, J.M.S. Cabral, Bioreactor design for clinical-grade expansion of stem cells, Biotechnol. J. 8 (2013) 644–654.
[7] H. Tavassoli, et al., Large-scale production of stem cells utilizing microcarriers: a biomaterials engineering perspective from academic research to commercialized products, Biomaterials 181 (2018) 333–346.
[8] T.S. Kaminski, O. Scheler, P. Garstecki, Droplet microfluidics for microbiology: techniques, applications and challenges, Lab Chip 16 (2016) 2168–2187.
[9] N. Shembekar, C. Chaipan, R. Utharala, C.A. Merten, Droplet-based microfluidics in drug discovery, transcriptomics and high-throughput molecular genetics, Lab Chip 16 (2016) 1314–1331.
[10] D. Kong, L. Peng, S. di Cio, P. Novak, J.E. Gautrot, Stem cell expansion and fate decision on liquid substrates are regulated by self-assembled nanosheets, ACS Nano 12 (2018) 9206–9213.
[11] F. Guilak, et al., Control of stem cell fate by physical interactions with the extracellular matrix, Cell Stem Cell 5 (2009) 17–26.
[12] D.E. Discher, D.J. Mooney, P.W. Zandstra, Growth factors, matrices, and forces combine and control stem cells, Science 324 (2009) 1673–1677.
[13] D. Kong, et al., Protein nanosheet mechanics controls cell adhesion and expansion on low-viscosity liquids, Nano Lett. 18 (2018) 1946–1951.
[14] X. Jia, et al., Adaptive liquid interfacially assembled protein nanosheets for guiding mesenchymal stem cell fate, Adv. Mater. (2019) 1905942.
[15] M.P. Hanga, et al., Expansion of human mesenchymal stem/stromal cells on temporary liquid microcarriers, J. Chem. Technol. Biotechnol. (2020), https://doi.org/10.1002/jctb.6601.
[16] D. Kong, K.D.Q. Nguyen, W. Megone, L. Peng, J.E. Gautrot, The culture of HaCaT cells on liquid substrates is mediated by a mechanically strong liquid-liquid interface, Faraday Discuss 204 (2017) 367–381.
[17] A.J. Engler, S. Sen, H.L. Sweeney, D.E. Discher, Matrix elasticity directs stem cell lineage specification, Cell 126 (2006) 677–689.
[18] B. Trappmann, et al., Extracellular matrix tethering regulates stem cell fate, Nat. Mater. 11 (2012) 642–649.
[19] C.R. Keese, I. Giaever, Cell growth on liquid interfaces: role of surface active compounds, Proc. Natl. Acad. Sci. Unit. States Am. 80 (1983) 5622–5626.
[20] W. Megone, D. Kong, L. Peng, J.E. Gautrot, Extreme reversal in mechanical anisotropy in liquid-liquid interfaces reinforced with self-assembled protein nanosheets, J. Colloid Interface Sci. 594 (2021) 650–657.
[21] O. Chaudhuri, et al., Substrate stress relaxation regulates cell spreading, Nat. Commun. 6 (2015) 6365.
[22] O. Chaudhuri, et al., Hydrogels with tunable stress relaxation regulate stem cell fate and activity, Nat. Mater. 15 (2016) 326–334.

[23] M. Bennett, et al., Molecular clutch drives cell response to surface viscosity, Proc. Natl. Acad. Sci. Unit. States Am. 115 (2018) 1192–1197.
[24] M. Cantini, H. Donnelly, M.J. Dalby, M. Salmeron-Sanchez, The plot thickens: the emerging role of matrix viscosity in cell mechanotransduction, Adv. Healthcare Mater. 9 (2019) 1901259.
[25] N. Denkov, S. Tcholakova, I. Lesov, D. Cholakova, S.K. Smoukov, Self-shaping of oil droplets via the formation of intermediate rotator phases upon cooling, Nature 528 (2015) 392–395.
[26] A. Zarbakhsh, J. Bowers, J.R.P. Webster, A new approach for measuring neutron reflection from a liquid/liquid interface, Meas. Sci. Technol. 10 (1999) 738–743.
[27] M. Campana, et al., Adsorption of bovine serum albumin (BSA) at the oil/water interface: a neutron reflection study, Langmuir 31 (2015) 5614–5622.
[28] P.A. Gunning, et al., Effect of surfactant type on surfactant-protein interactions at the air-water interface, Biomacromolecules 5 (2004) 984–991.
[29] R.V. Mannige, et al., Peptoid nanosheets exhibit a new secondary-structure motif, Nature 526 (2015) 415–420.
[30] Q. Liu, et al., Cofactor-free oxidase-mimetic nanomaterials from self-assembled histidine-rich peptides, Nat. Mater. (2020), https://doi.org/10.1038/s41563-41020-00856-41566.
[31] M.A. Creighton, Y. Ohata, J. Miyawaki, A. Bose, R.H. Hurt, Two-dimensional materials as emulsion stabilizers: interfacial thermodynamics and molecular barrier properties, Langmuir 30 (2014) 3687–3696.
[32] R. Oria, et al., Force loading explains spatial sensing of ligands by cells, Nature 552 (2017) 219–224.
[33] L. Blanchoin, R. Boujemaa-Paterski, C. Sykes, J. Plastino, Actin dynamics, architecture, and mechanics in cell motility, Physiol. Rev. 94 (2014) 235–263.
[34] J. Liu, et al., Talin determines the nanoscale architecture of focal adhesions, Proc. Natl. Acad. Sci. Unit. States Am. (2015) E4864–E4873.
[35] W.R. Legant, et al., Multidimensional traction force microscopy reveals out-of-plane rotational moments about focal adhesions, Proc. Natl. Acad. Sci. Unit. States Am. 110 (2013) 881–886.
[36] J. Connelly, et al., Actin and SRF transduce physical cues from the microenvironment to regulate epidermal stem cell fate decisions, Nat. Cell Biol. 12 (2010) 711–718.
[37] K.B. Jensen, F.M. Watt, Single-cell expression profiling of human epidermal stem and transit-amplifying cell: lrig1 is a regulator of stem cell quiescence, Proc. Natl. Acad. Sci. Unit. States Am. 103 (2006) 11958–11963.
[38] J.E. Gautrot, et al., The nanoscale geometrical maturation of focal adhesions controls stem cell differentiation and mechanotransduction, Nano Lett. 14 (2014) 3945–3952.
[39] M.D. Treiser, et al., Cytoskeleton-based forecasting of stem cell lineage fates, Proc. Natl. Acad. Sci. Unit. States Am. 107 (2010) 610–615.
[40] L. Peng, J. Gautrot, Long term expansion profile of mesenchymal stromal cells at protein nanosheet-stabilised bioemulsions for next generation cell culture microcarriers, Mater. Today Bio 12 (2021) 100159.